

# Results of a Search for Paraphotons with Intense X-ray Beams at SPring-8

T. Inada<sup>a</sup>, T. Namba<sup>b</sup>, S. Asai<sup>a</sup>, T. Kobayashi<sup>b</sup>,  
Y. Tanaka<sup>c</sup>, K. Tamasaku<sup>c</sup>, K. Sawada<sup>c</sup>, T. Ishikawa<sup>c</sup>

<sup>a</sup>*Department of Physics, Graduate School of Science, the University of Tokyo, 7-3-1 Hongo, Bunkyo, Tokyo 113-0033, Japan*

<sup>b</sup>*International Center for Elementary Particle Physics, the University of Tokyo, 7-3-1 Hongo, Bunkyo, Tokyo 113-0033, Japan*

<sup>c</sup>*Spring-8/RIKEN Harima Institute, 1-1-1 Kouto, Sayo-cho, Sayo-gun, Hyogo 679-5148, Japan*

---

## Abstract

A search for paraphotons, or hidden  $U(1)$  gauge bosons, is performed using an intense X-ray beamline at SPring-8. “Light Shining through a Wall” technique is used in this search. No excess of events above background is observed. A stringent constraint is obtained on the photon–paraphoton mixing angle,  $\chi < 8.06 \times 10^{-5}$  (95% C.L.) for  $0.04 \text{ eV} < m_{\gamma'} < 26 \text{ keV}$ .

---

## 1. Introduction

Paraphotons, or hidden sector photons are gauge bosons of hypothetical  $U(1)$  symmetry. Many extensions of the Standard Model predict such a symmetry [1]. Some of them also predict tiny mixing of paraphotons with ordinary photons through very massive particles which have both electric and hidden charge [2]. This effective mixing term induces flavor oscillations between paraphotons and ordinary photons [3]. With this oscillation mechanism, a high sensitive search can be done with a method called “Light Shining through a Wall (LSW)” technique[4], in which incident photons oscillate into paraphotons that are able to pass through a wall and oscillate back into photons.

Recently, a detailed theoretical calculation has been performed for axion LSW experiment[5]. Since both axion– and paraphoton–conversion are described as the same quantum oscillations, the conversion probability for axions can be interpreted as that of paraphotons by replacing parameters from  $\frac{\beta\omega}{m^2}$  to  $\chi$  in Eq. (29) in [5]. After propagation in vacuum for length  $L$ , the probability

---

*Email address:* tinada@icepp.s.u-tokyo.ac.jp (T. Inada)

of converting a paraphoton into a photon (or vice versa) is given by,

$$p_{\gamma \leftrightarrow \gamma'}(L) = \left( \frac{\omega + \sqrt{\omega^2 - m_{\gamma'}^2}}{\sqrt{\omega^2 - m_{\gamma'}^2}} \chi \right)^2 \sin^2 \left( \frac{L}{2} \left( \omega - \sqrt{\omega^2 - m_{\gamma'}^2} \right) \right), \quad (1)$$

where  $\chi$  is the mixing angle,  $m_{\gamma'}$  is the mass of the paraphoton, and  $\omega$  is the energy of photon. For low mass region ( $m_{\gamma'} \ll \omega$ ), it becomes a well-known expression of a neutrino-like oscillation;  $p_{\gamma \leftrightarrow \gamma'}(L) = 4\chi^2 \sin^2(m_{\gamma'}^2 L / 4\omega)$ .

Searches have been performed with this LSW technique by using optical photons [6] or microwave photons [7], without any evidence. Useful summary papers are available (see *e.g.* [8]). For an axion-LSW search, an experiment using X-rays has been performed at ESRF[9].

In this letter, we report a new search for paraphotons with the LSW method. We use an intense X-ray beam created by a long undulator at SPring-8 synchrotron radiation facility to search paraphotons whose mass is in the ( $10^{-1}$ – $10^4$ ) eV region.

## 2. Experimental Setup

BL19LXU [10] beamline at SPring-8 (Fig. 1) is used for X-ray source. A 30-m long undulator is placed on the electron storage ring as shown in Fig. 1. A bunch length of electrons in the storage ring is 40 ps, and a bunch interval is 23.6 ns. Structure of a X-ray beam represents the bunch structure of electrons, but we regard it as a continuous beam because time resolution of X-ray detector is larger than this structure. An energy of the X-ray beam is tunable between 7.2 and 18 keV by changing a gap width of the undulator. Higher energy of its 3rd harmonics (21.6 ~ 51 keV) is also available. X-ray beam is monochromated with a Si(111) double crystal monochromator to the level of  $\Delta\omega/\omega \sim 10^{-4}$ . A reflection angle is determined from Bragg condition, and is typically  $\sim 100$  mrad for energies we use. A beam size is about 1 mm, and a vertical profile ( $\rho(x)$ ) is measured with a slit with 10  $\mu\text{m}$  pitch. Shape of  $\rho(x)$  is similar to Gaussian whose FWHM is 383  $\mu\text{m}$ .

From the monochromator, the X-ray beam is guided through vacuum tubes, whose length is about 3.5 m. Tubes are evacuated better than  $4 \times 10^{-5}$  Pa, and a double mirror is placed at the downstream edge of the tube. These mirrors are adjusted for the total reflection, and their reflection angle is tuned at 3.0 mrad (or 2.0 mrad) during our search (only at 26 keV search). They serve as a beam-pass filter, since only X-ray beams satisfying a severe condition of total reflection are bounced up and the other off-axis background photons are blocked. The X-ray beam changes its path with these mirrors and only the reflected beam is selected with a slit, and guided to the X-ray detector.

Two beam shutters are placed in the beamline. Main Beam Shutter (MBS) is placed just before the monochromator, and DownStream Shutter (DSS) is placed between the monochromator and the mirrors. Photon changes into paraphoton in a vacuum tube between the monochromator and DSS, and then changes back

inversely in the region between DSS and the mirrors. Each length at the beam center is  $(277 \pm 2)$  cm and  $(65.4 \pm 0.5)$  cm, respectively.

A germanium detector (Canberra BE2825) is used to detect X-ray signal. A diameter and thickness of its crystal is 60 mm and 25 mm, respectively. Signal of Ge detector is shaped with an amplifier (ORTEC 572) and recorded by a peak hold ADC (HOSHIN C-011). Energy resolution of the detector is measured with  $^{55}\text{Fe}$ ,  $^{68}\text{Ge}$ ,  $^{57}\text{Co}$ , and  $^{241}\text{Am}$  sources, and typical energy resolution at 10 keV is 0.17 keV ( $\sigma$ : standard deviation). Absolute efficiencies of the X-ray detector ( $\epsilon$ ) are also measured by the same sources. Measured efficiencies are consistent with GEANT4 Monte Carlo results, which includes all attenuations in the air, carbon composite window (thickness = 600  $\mu\text{m}$ ) of the detector, and surface dead layer (thickness =  $(7.7 \pm 0.9)$   $\mu\text{m}$ ) of the germanium crystal.

The detector is shielded by lead blocks whose thickness is about 50 mm except for a collimator on the beam axis whose hole diameter is 30 mm, much larger than the X-ray beam size. The position of the collimator and the germanium crystal against the beam is adjusted by using a photosensitive paper which is sensitive to the X-ray.

After the monochromator reaches thermal equilibrium, beam flux becomes stable. Absolute flux of the X-ray beam and its stability are monitored by a silicon PIN photodiode (Hamamatsu S3590-09, thickness = 300  $\mu\text{m}$ ). This photodiode is inserted in front of the collimator of the lead shield, and DSS is opened for the flux measurement. During this measurement, the collimator hole is closed to avoid the radiation damage to the germanium detector. The energy deposited on the PIN photodiode is calculated using its output current and the W-value of silicon ( $W = 3.66$  eV). Fraction of the X-ray energy deposition in the PIN photodiode is computed with GEANT4 simulation for each energy. To correct the saturation effect of the PIN photodiode, thin aluminum foils are inserted before the photodiode to attenuate X-ray flux. Attenuation coefficient of aluminum is also checked by GEANT4 simulation. The flux can be measured with an accuracy of less than 5%.

### 3. Measurement and Analysis

A paraxial search is performed from 14th to 20th June, 2012. 9 measurements are performed with different X-ray energies from 7.27 keV to 26.00 keV. Results are summarized in Tab. 1. Beam intensities ( $I$ ) are monitored every 3–4 hours by the PIN photodiode as described in the previous section. Time drifts of the beam flux ( $< 10\%$ ) are confirmed only at the beginning of the measurement since, due to heavy heat load, it takes about 30 minutes for experimental setup to become thermally stable. Fluxes which get well-stabilized in the thermal equilibrium are listed and used for the analysis. Energy calibration of the detector is also performed every 3–4 hours with a  $^{57}\text{Co}$  source.

---

In this paper, all error values represent 1 sigma.

BG spectrum (Fig. 2 (a)) is measured from 16th to 17th June with MBS closed. The other setup including the lead shields are completely the same as in the paraphoton searches. Total livetime of BG measurement is  $1.6 \times 10^5$  s. The BG rate at 7.00 keV is  $(10.9 \pm 0.3) \times 10^{-3} \text{ s}^{-1} \text{ keV}^{-1}$  and gradually decreases toward  $(4.6 \pm 0.2) \times 10^{-3} \text{ s}^{-1} \text{ keV}^{-1}$  at 26.00 keV. No apparent structure is observed in the measured BG spectrum except for 10.6 keV and 12.6 keV, X-rays from the lead shields.

We define signal region as inside  $\pm 2\sigma$  around the beam energy  $\omega$ . Since signal regions are not overlapped among all measurements, the BG spectrum is commonly used for all subtractions (Fig. 2 (b)). The subtracted signal rates ( $\Delta N$ ) are also shown in Tab. 1, and no significant excess is observed for all 9 measurements. Using these rates, we set upper limits on signal rates of measurements. Gaussian distributions are assumed from center values and the standard deviations of  $\Delta N$ , and 95% C.L. positions in the physical (i.e. positive) regions are set as a signal upper limit ( $\Delta N_{95}$ ). Finally, the upper limits on the LSW probability ( $P_{95}$ ) are obtained by  $\Delta N_{95}/\epsilon I$ .

To translate  $P_{95}$  to the limit on the mixing parameter  $\chi$ , we need to consider  $\rho(x)$  of the X-ray beam. Since the incident angles of the beam into the second crystal of the monochromator and the first mirror are very shallow,  $\rho(x)$  affects the lengths of the oscillation regions. As a result, these lengths are smeared by  $\rho(x)$ , and the LSW probability is written as,

$$P = \int_x \rho(x) p_{\gamma \rightarrow \gamma'}(L_1(x)) p_{\gamma' \rightarrow \gamma}(L_2(x)) dx. \quad (2)$$

Here,  $L_1(x)$  is the length of photon  $\rightarrow$  paraphoton oscillation region modified by the vertical position, and  $L_2(x)$  is that of the re-oscillation region. The integration is numerically calculated for each  $\omega$  as a function of  $m_{\gamma'}$ , and  $P_{95}$  is translated to the limit on  $\chi$ . Figure 3 shows 95% C.L. limit obtained using a data set of 9.00 keV measurement, and upper side of the line is excluded. The limit is smoothed by the smearing effect of  $\rho(x)$  and becomes constant for masses from 5 eV up to around 9 keV (labeled as “(b)”).

Limit oscillations in the region (a) are ruled out by the combination of 9 measurements. Combined results are obtained by the described procedure using  $\chi^4$  distributions and multiplying each others. 95% C.L. upper limit of the combined result is shown in Fig. 4 with other results. The worst value of  $\chi_{\text{worst}} = 8.01 \times 10^{-5}$  appears at 1.39 eV. Systematic errors on energy scale of the detector and oscillation region lengths, including contribution from the uncertainty of  $\rho(x)$  ( $\Delta L < 0.5$  mm), are estimated by varying the parameters and obtained to be  $\Delta\chi_{\text{worst}}/\chi_{\text{worst}} = {}^{+0.52}_{-0.15}$  %. Conservatively,  $\chi_{\text{worst}} + \Delta\chi_{\text{worst}}$  represents our final result,

$$\chi < 8.06 \times 10^{-5} \quad (95\% \text{ C.L.}). \quad (3)$$

This result is valid for masses up to 26 keV, the maximum beam energy of our search. Our result is the most stringent for masses around eV region as a terrestrial search.

#### 4. Conclusion

A paraphoton search is performed at BL19LXU beamline in SPring-8 synchrotron radiation facility. A double oscillation process, “photons oscillating into paraphotons and oscillating back into photons”, is assumed, and photons passing through a wall are searched. No such photons are observed, and a new limit on the photon–paraphoton mixing angle,  $\chi < 8.06 \times 10^{-5}$  (95% C.L.) is obtained for  $0.04 \text{ eV} < m_{\gamma'} < 26 \text{ keV}$ .

#### Acknowledgements

The synchrotron radiation experiment is performed at BL19LXU in SPring-8 with the approval of RIKEN (Proposal No. 20120088). Sincere gratitude is also expressed to Dr. Suehara and Mr. Ishida for useful discussions. Work of T. Inada is supported in part by Advanced Leading Graduate Course for Photon Science (ALPS) at U. Tokyo.

#### References

- [1] J. Jaeckel and A. Ringwald, *Ann. Rev. Nucl. Part. Sci.* 60(2010)405.
- [2] B. Holdom, *Phys. Lett. B* 166(1986)196.
- [3] L. B. Okun, *JETP* 56(1982)502.
- [4] K. Van Bibber *et al.*, *Phys. Rev. Lett.* 59(1987)759.
- [5] S. L. Adler *et al.*, *Ann. Phys.* 323(2008)2851.
- [6] BFRT Collaboration, R. Cameron *et al.*, *Phys. Rev. D* 47(1993)3707; BMV Collaboration, M. Fouche *et al.*, *Phys. Rev. D* 78(2008)032013; GammeV Collaboration, A. Chou *et al.*, *Phys. Rev. Lett.* 100(2008)080402; LIPPS Collaboration, A. Afanasev *et al.*, *Phys. Lett. B* 679(2009)317; ALPS Collaboration, K. Ehret *et al.*, *Phys. Lett. B* 689(2010)149.
- [7] ADMX Collaboration, A. Wagner *et al.*, *Phys. Rev. Lett.* 105(2010)171801; M. Betz and F. Caspers, *Conf. Proc. C* 1205201(2012)3320.
- [8] A. Ringwald, *Dark Universe* 1(2012)116.
- [9] R. Battesti *et al.*, *Phys. Rev. Lett.* 105(2012)250405.
- [10] M. Yabashi *et al.*, *Nucl. Instrum. Meth. A* 467-468(2001)678.
- [11] R. G. Beausoleil *et al.*, *Phys. Rev. A* 35(1987)4878.
- [12] E. R. Williams, J. E. Faller and H. A. Hill. *Phys. Rev. Lett.* 26(1971)721.

Side view

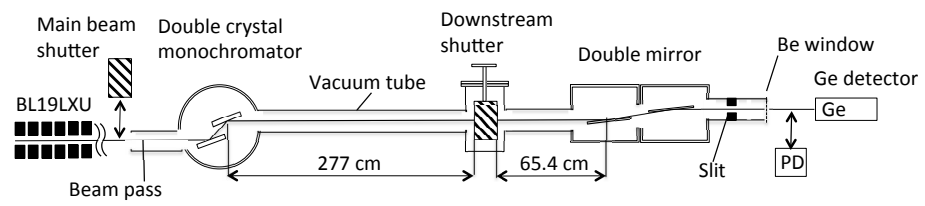


Figure 1: Schematic view of our experimental setup.

beam energy $\omega$ (keV)	livetime ( $10^4$ s)	detector resolution $\sigma$ (keV)	event rate in $(\omega \pm 2\sigma)$ $N$ ( $10^{-3} \text{ s}^{-1}$ )	BG subtracted rate in $(\omega \pm 2\sigma)$ $\Delta N$ ( $10^{-4} \text{ s}^{-1}$ )	signal upper limit $\Delta N_{95}$ ( $10^{-4} \text{ s}^{-1}$ )	beam flux $I$ ( $10^{13} \text{ s}^{-1}$ )	detector efficiency $\epsilon$ (%)	LSW prob. upper limit $P_{95}$ ( $10^{-16}$ )
7.27	2.5	0.16	$7.0 \pm 0.5$	$-0.9 \pm 5.7$	11.0	7.6	23	0.63
8.00	2.0	0.16	$6.5 \pm 0.6$	$-3.8 \pm 6.1$	10.3	8.9	33	0.35
9.00	3.2	0.17	$5.3 \pm 0.4$	$-7.6 \pm 4.5$	5.5	8.3	46	0.14
15.00	1.9	0.18	$4.2 \pm 0.5$	$-3.4 \pm 5.0$	8.2	4.6	51	0.35
16.00	2.1	0.18	$4.2 \pm 0.4$	$-3.1 \pm 4.8$	7.9	3.7	56	0.38
17.00	2.5	0.18	$4.2 \pm 0.4$	$-2.1 \pm 4.5$	7.8	2.3	61	0.56
21.83	2.5	0.19	$4.2 \pm 0.4$	$+4.2 \pm 4.3$	12.2	0.72	76	2.2
23.00	2.0	0.20	$3.9 \pm 0.4$	$+1.2 \pm 4.7$	10.5	0.43	78	3.1
26.00	2.6	0.21	$4.8 \pm 0.4$	$+7.6 \pm 4.6$	15.6	1.3	83	1.4

Table 1: Summary of 9 measurements of the paraphoton search. Errors are one standard deviation statistical errors.

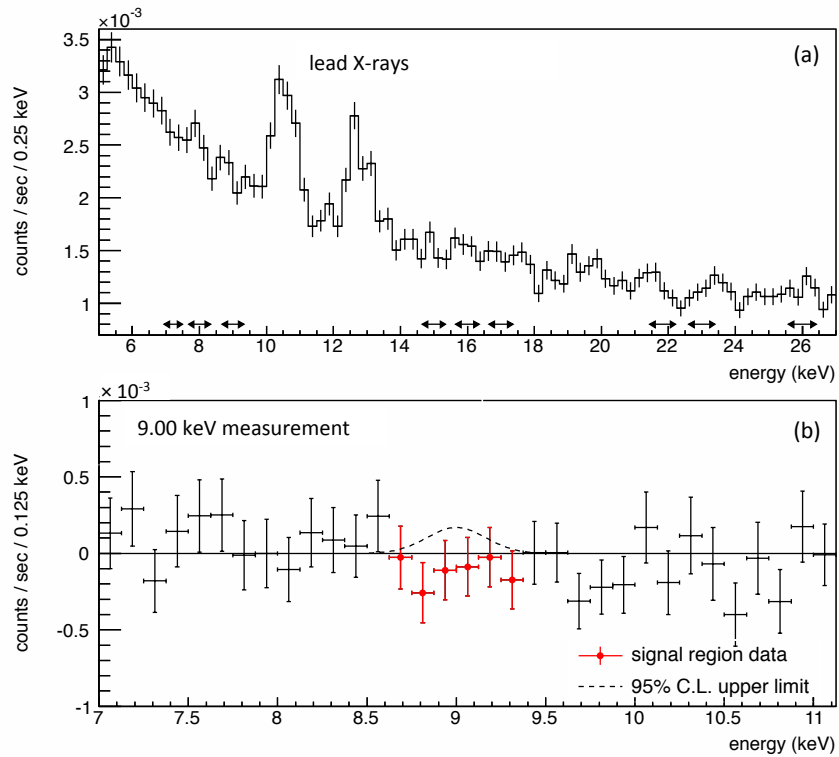


Figure 2: (a) Energy spectrum obtained with MBS closed (BG spectrum). Arrows show regions in which paraphoton searches are performed. (b) Energy spectrum measured at  $\omega = 9.00$  keV. Background contributions are subtracted using the spectrum (a). Signals with statistical errors are shown in cross, and dotted line shows obtained upper limit (95% C.L.) of the signal.



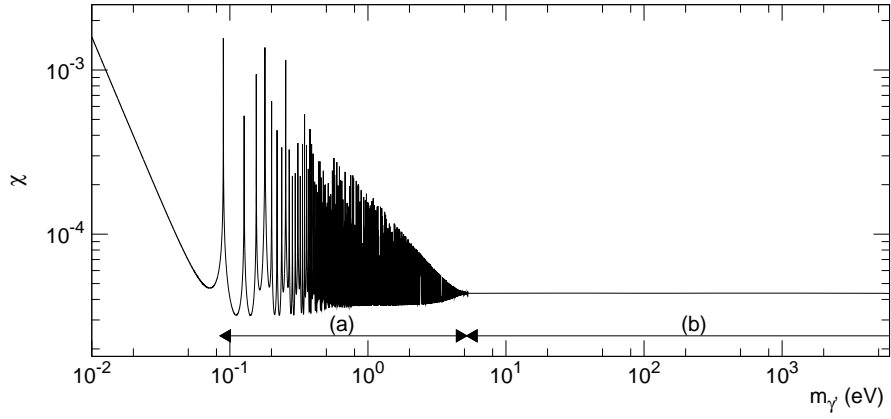


Figure 3: Upper limit (95% C.L.) on  $\chi$  as a function of paraphoton mass ( $m_{\gamma'}$ ) obtained with only one search at  $\omega = 9.00$  keV. Spiky structure is due to the photon–paraphoton oscillation as shown in Formula (1). Spikes are smeared for heavier mass region (labeled as “(b)”), because of the smearing effect in Formula (2).

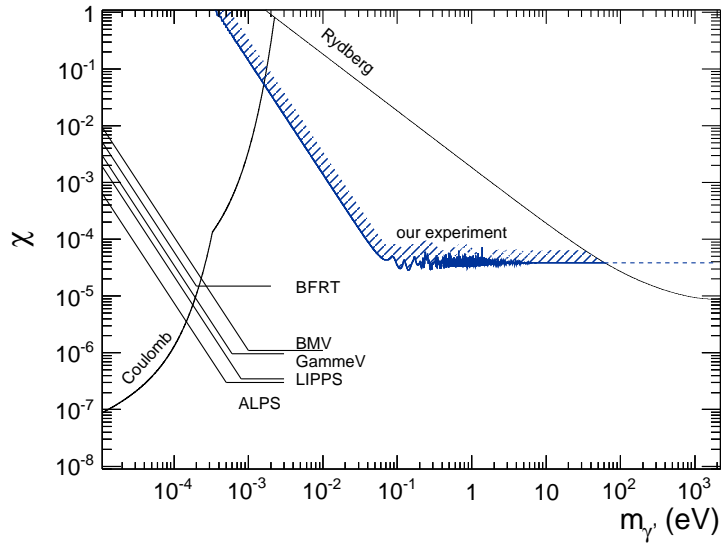


Figure 4: Obtained 95% C.L. limit on the paraphoton mixing angle compared with other laboratory experiments. Rydberg is a limit from the measurement of Rydberg atoms [11], Coulomb is from the Coulomb low confirmation [12], and BFRT, BMV, GammeV, LIPPS, and ALPS are from LSW experiments using optical laser [6].